Broken magnetic symmetry due to charge-order ferroelectricity discovered in (TMTTF)2X salts by multifrequency ESR

S. Yasin, B. Salameh, E. Rose, M. Dumm, Hans-Albrecht Krug von Nidda, Alois Loidl, M. Ozerov, G. Untereiner, L. Montgomery, Martin Dressel

Angaben zur Veröffentlichung / Publication details:

Yasin, S., B. Salameh, E. Rose, M. Dumm, Hans-Albrecht Krug von Nidda, Alois Loidl, M. Ozerov, G. Untereiner, L. Montgomery, and Martin Dressel. 2012. "Broken magnetic symmetry due to charge-order ferroelectricity discovered in (TMTTF)2X salts by multifrequency ESR." *Physical Review B* 85 (14): 144428. https://doi.org/10.1103/physrevb.85.144428.

Broken magnetic symmetry due to charge-order ferroelectricity discovered in $(TMTTF)_2X$ salts by multifrequency ESR

S. Yasin,[1,2] B. Salameh,[1,3] E. Rose,[1] M. Dumm,[1] H.-A. Krug von Nidda,[4] A. Loidl,[4] M. Ozerov,[2] G. Untereiner,[1] L. Montgomery,[5] and M. Dressel[1]

[1]*1. Physikalisches Institut, Universität Stuttgart, Pfaffenwaldring 57, 70550 Stuttgart, Germany*

[2]*Hochfeld-Magnetlabor Dresden, Helmholtz-Zentrum Dresden-Rossendorf, 01314 Dresden, Germany*

[3]*Department of Applied Physics, Tafila Technical University, Tafila, Jordan*

[4]*Experimentalphysik V, Center for Electronic Correlations and Magnetism, Universität Augsburg, 86135 Augsburg, Germany*

[5]*Department of Chemistry, Indiana University, Bloomington, 47405 Indiana, USA*

(Received 17 October 2011; revised manuscript received 6 February 2012; published 26 April 2012)

We have investigated the charge-ordered state of the quasi-one-dimensional organic charge-transfer salts $(TMTTF)_2X$ (where TMTTF stands for tetramethyltetrathiafulvalene and $X = PF_6$ AsF_6, SbF_6, and SCN) by performing comprehensive electron-spin-resonance (ESR) experiments at several frequencies for $4\ K < T < 300\ K$. At elevated temperatures all compounds show a linear increase of $\Delta H(T)$. Below the charge-ordering transition T_{CO} important anomalies are observed in both the temperature dependence and the anisotropy of the ESR linewidth. In the case of the centrosymmetric anions PF_6, AsF_6, and SbF_6, the linewidth doubles its periodicity when rotated in a plane normal to the molecule axis; and it exhibits a significant frequency dependence. This enhanced linewidth is caused by anisotropic Zeeman interaction that we identify as a relaxation process in the charge-ordered state where magnetically inequivalent sites are present in adjacent stacks. Thus, charge order not only produces ferroelectricity but also breaks the symmetry of the magnetic degree of freedom in these organic quantum spin chains. For $(TMTTF)_2SCN$ charge order coincides with the ordering of the non-centrosymmetric anions; the large contribution of dipolar interaction dominates the relaxation process.

DOI: 10.1103/PhysRevB.85.144428 PACS number(s): 75.10.Pq, 71.70.Ej, 75.25.−j, 76.30.−v

I. INTRODUCTION

The organic linear-chain compounds of the $(TMTSF)_2X$ and $(TMTTF)_2X$ family, where TMTSF and TMTTF denote tetramethyltetraselenafulvalene and tetramethyltetrathiafulvalene, respectively, and X stands for a monovalent anion such as SbF_6, AsF_6, PF_6, Br, and SCN, are considered to be benchmark systems for low-dimensional matter, which allow for exploration of interesting physics ranging from Mott insulator to Luttinger liquid.[1–4] Of particular importance are the transitions to various ordered ground states that develop in one-dimensional electron systems depending on the interplay of lattice, charge, and spin degrees of freedom.[5] The quasi-one-dimensional electronic behavior of $(TMTTF)_2X$ salts originates in their crystallographic structure. The planar TMTTF molecules stack in a slight zigzag configuration along the a axis that constitutes the highest conducting direction. With some minor interaction between the stacks they form layers in the ab plane which alternate with the anions X along the c axis (Fig. 1). Recently, it was pointed out that the contacts between the anions and the organic molecules via the methyl groups and the sulfur atoms are important and shall not be neglected when considering the charge-order transition.[6–9] Furthermore, the molecular stacks are not homogeneous, but the TMTTF molecules form dimers with important consequences on the electronic properties of these salts.[8] The $\frac{3}{4}$-filled conduction band ($\frac{1}{4}$-filled hole band) is split and becomes effectively half filled; dimerization also enhances the phenomenon of charge localization. Due to their small transfer integrals and strong on-site Coulomb repulsion TMTTF salts are Mott-Hubbard insulators.[10–12]

The quasi-one-dimensional systems with $\frac{1}{4}$-filled bands, where electronic correlations tend to localize the charge carriers along the chains, commonly exhibit a charge-ordering transition in the temperature range from 100 K to 200 K. Charge order (CO) in $(TMTTF)_2X$ salts has been intensively studied in the last decade.[6,9,13–27] The metal-insulator transition at $T_{CO} = 155$ K was first identified by a clear anomaly in the thermopower data of $(TMTTF)_2SbF_6$. The same transport anomaly was also recorded in $(TMTTF)_2AsF_6$ at about 100 K; and doping studies ensured that these are actually the same type of transition.[28] Resistivity measurements reveal a steep increase in the conductivity gap at T_{CO} for the three crystal directions of $(TMTTF)_2AsF_6$ (Refs. 25 and 6); this effect is even stronger for the two axes perpendicular to the stacks. Deuteration of the organic molecules of $(TMTTF)_2SbF_6$ and $(TMTTF)_2AsF_6$ enhances the CO transition temperature[24]; hydrostatic pressure reduces T_{CO}.[9]

Using one- and two-dimensional ^{13}C nuclear magnetic resonance (NMR) spectroscopy the phase transition was finally proven to be due to CO.[9,18,20,29] Subsequently, CO transitions were found in $(TMTTF)_2X$ ($X = PF_6$, AsF_6, SbF_6, ReO_4, and SCN) at 63 K, 102 K, 155 K, 227 K, and 160 K, respectively. Dielectric permittivity measurements[15–17] recognized the ferroelectric and antiferroelectric [in $(TMTTF)_2SCN$] order of the low-temperature ground states; CO is associated with a loss of the symmetry center for the molecules on the chain. The charge disproportionation can be locally probed by Raman and infrared vibrational spectroscopy.[30,31] Optical reflectivity measurements on $(TMTTF)_2AsF_6$ and $(TMTTF)_2PF_6$ with light polarized parallel to the molecular stacks (a axis) allowed us to detect a splitting of the electron-molecular-vibrational (emv) coupled intramolecular modes below the CO transition.[22,23] More sensitive are the asymmetric molecular vibrations along the molecule axis,[26] which are best measured perpendicular to the ab planes.[32,33]

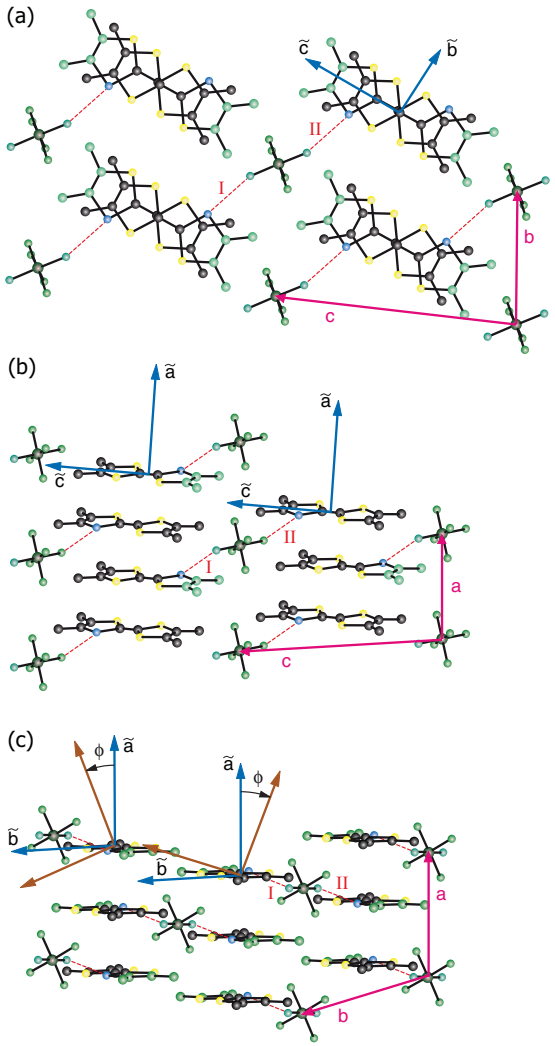

FIG. 1. (Color online) Crystal structure of $(TMTTF)_2SbF_6$ viewed (a) along the stacking direction a, (b) along the b axis, and (c) along the c direction. The TMTTF molecules are basically arranged in the direction $c + b$. The strongest couplings between the octahedral anions and the sulfur atoms are indicated by the red dashed lines I and II, which are related by inversion symmetry for $T > T_{CO}$. In the charge-ordered state, not only do the TMTTF molecules develop a charge disproportionation with alternating charge-rich and charge-poor molecules along the stacks, the anions also are slightly deformed. The inversion symmetry is lifted and contact I becomes shorter than contact II. Also shown is the configuration between the TMTTF molecular structure and the principal axes of the **g** tensor. At elevated temperatures the **g** tensor (blue arrows indicate the principal magnetic directions $\tilde{a}$, $\tilde{b}$, and $\tilde{c}$) is determined by the molecular structure. The $\tilde{a}$ axis of the **g** tensor is normal to the molecular plane and basically along the stacking direction, while the $\tilde{c}$ axis points along to the longest molecule extension. For $T < T_{CO}$ the principal axes of the **g** tensor rotate around the $\tilde{c}$ axis by an angle ϕ in opposite directions, resulting in the brown arrows.

For $(TMTTF)_2SCN$ the antiferroelectric CO transition is accompanied by an anion ordering which corresponds to the appearance of $(0, \frac{1}{2}, \frac{1}{2})$ satellite reflections in x-ray measurements.[34] In the case of TMTTF salts with centrosymmetric anions, no such superstructure can be observed at the ferroelectric CO transition and thus for many years the CO transition was labeled a "structureless" phase transition.[8,12,28,35,36] Recent x-ray investigations on $(TMTTF)_2PF_6$ and $(TMTTF)_2SbF_6$ indicate a significant increase in mosaicity upon approaching the CO transition that indicates the development of domains with different arrangement of charge on the molecules and coupling to the anions.[37] Already ^{19}F NMR spectroscopy provided empirical evidence that the coupling of the electrons on the TMTTF molecules to the anions is crucial for the CO phase.[20] This picture was confirmed by recent optical investigations[33] that reveal changes in the methyl groups and hexaflourides upon charge ordering as well as modifications of low-lying lattice modes. The involvement of the underlying lattice was also seen in the change of the thermal expansion coefficient at the CO transition of $(TMTTF)_2AsF_6$ and $(TMTTF)_2PF_6$.[38] Further indications for a lattice displacement come from neutron-scattering experiments.[39]

In line with these observations, Furukawa *et al.* observed an anomalous temperature behavior of the **g** tensor with a continuous rotation of the principal axes around the a axis when T decreases from room temperature to 20 K.[40] It is assigned to the electrostatic interaction of the anions on the TMTTF orbitals that gets enhanced upon thermal contraction. Recently, they also investigated the spin dynamics of $(TMTTF)_2PF_6$ by pulsed-ESR spectroscopy.[41] Due to transverse magnetic interaction, the charge reorients before the ground state is reached, leading to magnetic fluctuations in the ab plane and an anomaly in the relaxation time.

The present study explores the CO state in the quasi-one-dimensional salts $(TMTTF)_2X$ ($X = PF_6$, AsF_6, SbF_6, and SCN) by performing detailed multifrequency electron spin resonance experiments. A significant change in the magnetic properties at T_{CO} indicates the coupling of charge, lattice, and spin degrees of freedom. CO driven by Coulomb repulsion modifies the interaction with the anions. Alternatively, the electrostatic potential of the anions changes the electronic wave functions on the TMTTF molecules, leading to a rotation of the **g** tensor in two different directions, depending on the coupling. The magnetic interaction of these nonequivalent stacks is the course of the anisotropic Zeeman interaction that becomes relevant in the CO state as a relaxation process for the centrosymmetric anions. Moreover, we present a detailed analysis of the temperature dependence of the ESR linewidth in the antiferromagnetic fluctuation region of the salts $(TMTTF)_2SbF_6$ and $(TMTTF)_2SCN$.

II. EXPERIMENTAL DETAILS

The electron spin resonance (ESR) spectra were carried out in a continuous-wave X-band spectrometer (Bruker ESP 300) at 9.5 GHz and a W-band spectrometer (Bruker Elexsys 680) at 95 GHz at Stuttgart University and a Q-band spectrometer (Bruker Elexsys 500) at 34 GHz at Augsburg University.[42] The temperature dependence of the ESR properties was measured down to $T = 4$ K by utilizing continuous-flow helium cryostats. Single crystals of $(TMTTF)_2PF_6$, $(TMTTF)_2AsF_6$, $(TMTTF)_2SbF_6$, and $(TMTTF)_2SCN$ were grown by the standard electrochemical growth procedure outlined previously in Ref. 43. The typical size of the single crystals used in the

TABLE I. Temperature of charge localization T_ρ, charge order T_{CO}, spin-Peierls transition T_{SP}, antiferromagnetic order T_N, and exchange constants J of the $(TMTTF)_2X$ salts under consideration ($X = PF_6$, SbF_6, AsF_6, and SCN) (Refs. 5,6,27,48–50).

Compound	T_ρ (K)	T_{CO} (K)	T_{SP} (K)	T_N (K)	J (K)
$(TMTTF)_2PF_6$	250	67	19		420
$(TMTTF)_2AsF_6$	250	102	13		410
$(TMTTF)_2SbF_6$	240	157		8	400
$(TMTTF)_2SCN$	250	160		7	460

X-band ESR measurements was $2 \times 0.5 \times 0.1$ mm^3, while very small samples of less than $0.4 \times 0.4 \times 0.05$ mm^3 were sufficient for the Q- and W-band ESR measurements in order to avoid any sample-size effect that can lead to a broadening of the linewidth.[44]

In the triclinic crystals, the TMTTF molecules are stacked approximately normal to the molecular plane in the a direction. The crystallographic b axis points toward adjacent stacks as can be seen in Fig. 1; the projection normal to a is commonly called b'. The TMTTF stacks are separated in the c direction by the anions X; c^* is the projection of the crystallographic c axis normal to the ab' plane. As pointed out previously,[40,45,46] the g factor measured by ESR experiments is determined by the π electronic wave function on the TMTTF molecule and the arrangement of the $\mathbf{g}$ tensor can be solely deduced from the molecular symmetry. Hence, we introduce a Cartesian coordinate system linked to the TMTTF molecule, which describes the principal axes of the $\mathbf{g}$ tensor.[47] Here $\tilde{a}$ is normal to the molecular $\tilde{b}\tilde{c}$ plane and $\tilde{c}$ denotes the long axis of the molecule, as is depicted in Fig. 1.

In our ESR experiments the crystals can be rotated around an axis perpendicular to the static magnetic field using a goniometer; the accuracy of the sample positioning was within 2°. The g value was determined by comparing the resonance field of the measured ESR signal with that of DPPH (2,2-diphenyl-1-picrylhydrazyl).

The characteristic temperatures of the $(TMTTF)_2X$ salts under investigation are summarized in Table I.

III. RESULTS

A. X-band investigations

In order to determine the principal magnetic axes of the single crystals, the angular dependence of the X-band ESR linewidth and g value was investigated at room temperature by rotating the single crystal around the three axes ($\tilde{a}$, $\tilde{b}$, and $\tilde{c}$). For all investigated salts the ESR spectra at elevated temperature are governed by the conduction electrons ($g \approx 2$). The single ESR line has a symmetric Lorentzian line shape for all orientations. In Fig. 2 we plot the angular dependence of the g value and the linewidth (half width at half maximum) when the $(TMTTF)_2SbF_6$ crystal, as an example, is rotated around the $\tilde{a}$ axis ($B_0 \parallel \tilde{b}\tilde{c}$ plane), the $\tilde{b}$ axis ($B_0 \parallel \tilde{a}\tilde{c}$ plane), and $\tilde{c}$ axis ($B_0 \parallel \tilde{a}\tilde{b}$ plane). The findings for the other TMTTF salts show the same angular dependencies; the obtained room-temperature values of the linewidth (ΔH) and the g shift ($\Delta g = g - 2.002\,319$) are listed in Table II.

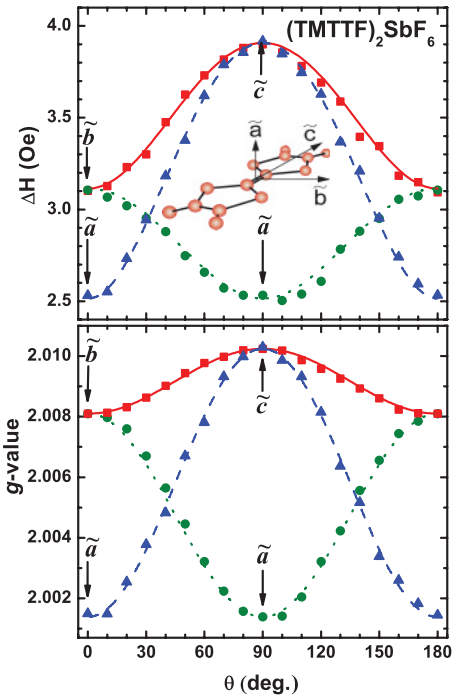

FIG. 2. (Color online) Angular dependence of the ESR linewidth ΔH (HWHM) (top), and the g value (bottom) of $(TMTTF)_2SbF_6$ at room temperature measured at X-band frequency when the static magnetic field B_0 is rotated within the $\tilde{a}\tilde{b}$ plane (green circles), the $\tilde{b}\tilde{c}$ plane (red squares), and the $\tilde{a}\tilde{c}$ plane (blue triangles). The least-squares fits of the linewidth and the g value by Eqs. (1) and (2) are shown by the corresponding lines. The inset demonstrates the orientation of the different orthogonal directions within the TMTTF molecule. The $\tilde{a}$ axis is normal to the plane, the $\tilde{c}$ axis points in the long direction, and $\tilde{b}$ points along the intermediate short direction.

For the chain direction (approximately the $\tilde{a}$ axis) the g value is close to that of a free electron. The linewidth and the g value exhibit the same anisotropy with the largest value along the $\tilde{c}$ axis and the smallest value along the $\tilde{a}$ axis. The angular dependence of the linewidth and the g value can be fitted by

$$\Delta H(\theta) = \left(\Delta H_{\min}^2 \cos^2\theta + \Delta H_{\max}^2 \sin^2\theta\right)^{1/2}, \quad (1)$$

$$g(\theta) = \left(g_{\min}^2 \cos^2\theta + g_{\max}^2 \sin^2\theta\right)^{1/2}, \quad (2)$$

TABLE II. ESR results for the four $(TMTTF)_2X$ salts obtained by X-band measurements at room temperature along the three principal axes of the $\mathbf{g}$ tensor, where $\tilde{a}$ is normal to the molecular and almost parallel to the stacking direction a, $\tilde{c}$ is directed along the extended axis of the TMTTF molecule, and $\tilde{b}$ is normal to both. ΔH stands for the linewidth (half width at half maximum) and Δg for the shift in g factor compared to the free electron value ($\Delta g = g - 2.002\,319$).

$(TMTTF)_2X$	Δg (10^{-3})			ΔH (Oe)		
$X =$	$\tilde{a}$	$\tilde{b}$	$\tilde{c}$	$\tilde{a}$	$\tilde{b}$	$\tilde{c}$
	directions			directions		
PF_6	−0.99	6.01	8.01	2.78	3.49	3.88
AsF_6	−1.04	6.12	8.10	2.63	3.09	4.09
SbF_6	−0.93	5.78	7.92	2.51	3.11	3.91
SCN	−1.04	6.00	7.87	2.87	3.49	4.43

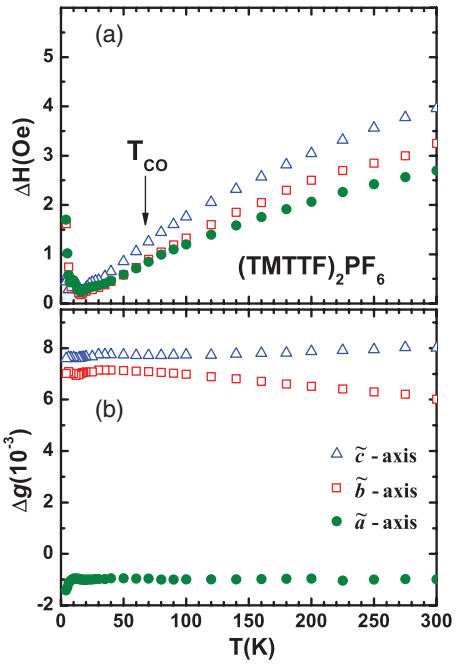

FIG. 3. (Color online) Temperature dependence of ESR parameters of $(TMTTF)_2PF_6$ measured by X-band spectroscopy along the three crystal orientations. (a) The linewidth ΔH and (b) the change in the g value obtained along the $\tilde{a}$ axis (green solid dots), the $\tilde{b}$ direction (open red squares), and the $\tilde{c}$ direction (blue triangles). Basically no change in $\Delta H(T)$ and $\Delta g(T)$ is observed at the charge-ordering temperature $T_{CO} = 67$ K.

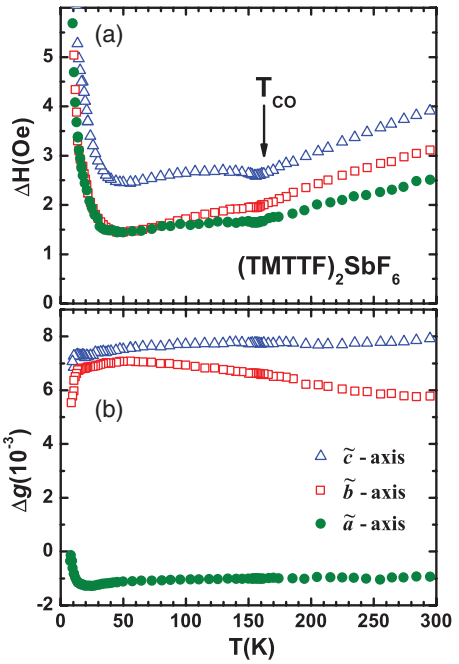

FIG. 4. (Color online) Temperature dependence of (a) the linewidth ΔH, and (b) the change in the g value for $(TMTTF)_2SbF_6$ measured by X-band ESR along the three crystal orientations. The green solid dots correspond to the $\tilde{a}$ axis, the open red squares indicate the $\tilde{b}$ direction, and the blue triangles are measured along the $\tilde{c}$ direction.

where ΔH_{min} (ΔH_{max}) and g_{min} (g_{max}) are the values along the $\tilde{a}$ axis ($\tilde{b}$ axis) determined by the measurements within the $\tilde{a}\tilde{b}$ plane, along the $\tilde{b}$ axis ($\tilde{c}$ axis) determined by the measurements within the $\tilde{b}\tilde{c}$ plane, and along the $\tilde{a}$ axis ($\tilde{c}$ axis) determined by the measurements within the $\tilde{a}\tilde{c}$ plane, respectively.

Our findings strongly indicate that the spin-phonon interaction is the dominant scattering process at high temperatures where the anisotropy in the g value arises from the spin-orbit coupling, that is, the coupling between the spin angular momentum and the orbital angular momentum of the conduction electron.[51,52] The spin angular momentum is always oriented parallel to the magnetic field, but the orbital angular momentum of the conduction electron, which is delocalized on the molecular orbitals, is locked to the molecular wave function. This implies that the eigendirections of the **g** tensor are solely deduced from the molecular symmetry; that is, for a planar molecule such as TMTTF the largest g value is observed when the static magnetic field B_0 is applied parallel to the long axis of the molecule ($\tilde{c}$ axis), the intermediate value is measured with a field applied parallel to the short axis of the molecule ($\tilde{b}$ axis), and the smallest when B_0 is perpendicular to the molecular plane ($\tilde{a}$ axis).

The temperature dependence of the X-band ESR results along the three principal magnetic directions is presented in Figs. 3 through 6 for the different $(TMTTF)_2X$ salts. Since the behavior of $(TMTTF)_2PF_6$ has been discussed previously,[49] here we start with the results obtained on $(TMTTF)_2SbF_6$ (Fig. 4) to point out the most important findings. In the high-temperature region ΔH exhibits a distinct anisotropy, as just discussed; it is largest along the $\tilde{c}$ axis and smallest along the $\tilde{a}$ axis. For all directions ΔH narrows linearly as the temperature is lowered down to the ordering temperature ($T_{CO} = 156$ K), where a clear anomaly in the linewidth is identified along all three directions. By reducing the temperature below T_{CO} the linewidth starts to decrease more slowly and its anisotropy begins to change. The g shift for the three main axes is basically temperature independent; it exhibits the same anisotropy as the linewidth. The values of Δg observed for the three axes are very small (see Table II). In the case of TMTSF salts Δg is about ten times larger due to the stronger spin orbit coupling of selenium.[45,50] Δg attains a negative value when the magnetic field is applied parallel to the stacking direction ($\tilde{a}$ axis) and a positive value when it is applied perpendicular to it ($\tilde{b}\tilde{c}$ plane). The anisotropy of the g factor between the $\tilde{b}$ and $\tilde{c}$ axes decreases slowly upon cooling. As displayed in Fig. 4, for all directions of $(TMTTF)_2SbF_6$ the linewidth begins to broaden as the temperature falls below 45 K; it changes slope at about 15 K before the ESR spectra in all three directions vanish totally at $T_N = 8$ K. This phase transition is accompanied by a decrease in the g shift for the $\tilde{b}$ and $\tilde{c}$ axes; along the $\tilde{a}$ axis the g factor becomes larger below $T \approx 15$ K.

For $(TMTTF)_2AsF_6$ the CO transition can be identified in all directions as a small dip in $\Delta H(T)$ at $T_{CO} = 102$ K, as depicted in Fig. 5. When the temperature is reduced below T_{CO}, the lines begin to narrow more slowly. No magnetic order develops in $(TMTTF)_2AsF_6$, as seen from the g factor, but the system undergoes a spin-Peierls transition at $T_{SP} = 13$ K, below which the spin susceptibility decreases rapidly upon reducing the temperature.[27] Below around 35 K, the width

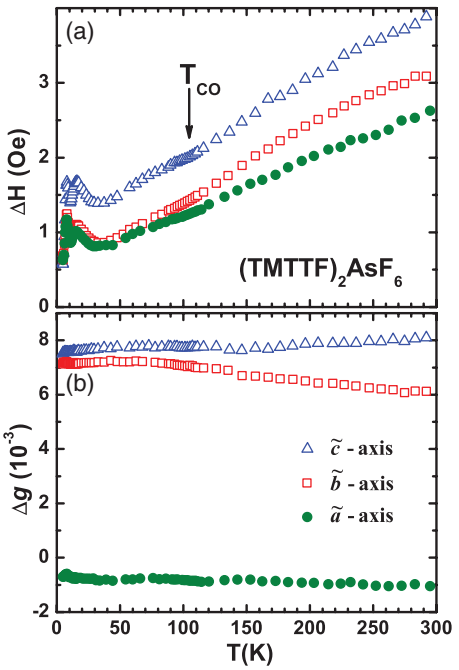

FIG. 5. (Color online) Temperature dependence of (a) the ESR linewidth ΔH and (b) the g shift $\Delta g(T) = g(T) - 2.002\,319$ for $(TMTTF)_2AsF_6$ measured by X-band spectroscopy along the three directions $\tilde{a}$ (green dots), $\tilde{b}$ (open red squares), and $\tilde{c}$ (blue triangles).

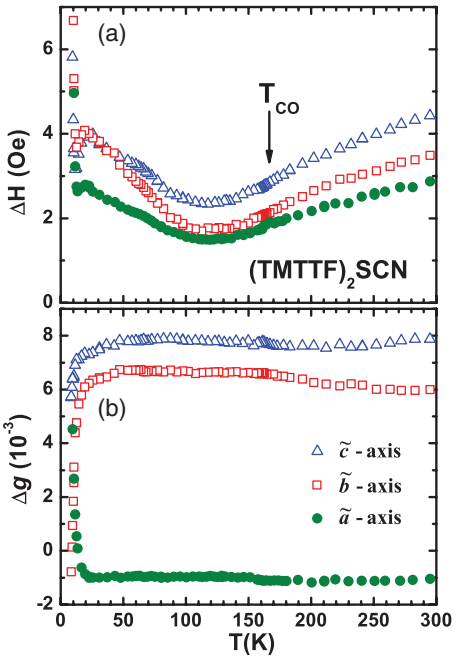

FIG. 6. (Color online) (a) ESR linewidth ΔH and (b) Δg of $(TMTTF)_2SCN$ measured in the X band as a function of temperature along the three principal directions as indicated.

starts to broaden strongly as T is reduced and for even lower temperatures ($T < 16$ K) strong fluctuations are observed.

In the case of $(TMTTF)_2SCN$, charge ordering at $T_{CO} = 160$ K also shows up in the linewidth as a minor hump. The g factors are not affected significantly by the CO, albeit minor anomalies can be identified at T_{CO}. With reducing the temperature further $\Delta H(T)$ goes through a broad minimum around 120 K and then increases down to $T \approx 20$ K; this behavior is similar along all three directions. At even lower temperatures a minimum of ΔH is detected around 13 K but then the linewidth increases strongly down to $T_N = 7$ K. The magnetic order is seen in all three directions and resembles the behavior observed in $(TMTTF)_2SbF_6$. This phase transition is accompanied by a strong negative shift of the g value for the $\tilde{b}$ and $\tilde{c}$ axes and a pronounced increase along the $\tilde{a}$ axis leading to a change in sign of Δg for $(TMTTF)_2SCN$.

Finally, we want to return to $(TMTTF)_2PF_6$; at elevated temperatures the ESR properties are similar to the other members of the TMTTF family. The data shown in Fig. 3 are taken from Ref. 49 and discussed there in more detail. The compound is particular in the sense that the CO phase transition at $T_{CO} = 67$ K basically does not show up in the ESR linewidth; hence, it can serve a reference system to model the background for $T > 80$ K. At low temperatures the linewidth increases due to the spin-Peierls transition at $T_{SP} = 19$ K. These data are listed in Table I.

B. Q- and W-band results

In order to gain a deeper insight into the anisotropic interaction, we have performed Q-band (34 GHz) and W-band (95 GHz) ESR measurements as a function of orientation and temperature. First, the principal magnetic axes of $(TMTTF)_2SbF_6$ and $(TMTTF)_2AsF_6$ were determined by angular-dependent room-temperature investigations. For all orientations the resulting Q- and W-band spectra reveal a symmetric Lorentzian line shape. Also, the angular dependence of ΔH and Δg were similar to our X-band results, as far as the absolute values and the anisotropy along the $\tilde{a}\tilde{c}$ and $\tilde{b}\tilde{c}$ planes are concerned. Only within the $\tilde{a}\tilde{b}$ plane does a pronounced frequency dependence show up in the CO state, which is considered in the following section. In Figs. 7 and 8 the W-band ESR linewidth and the g shift of $(TMTTF)_2SbF_6$ and $(TMTTF)_2AsF_6$ are plotted as a function of temperature for the three principal magnetic axes: $\tilde{a}$, $\tilde{b}$, and $\tilde{c}$. The corresponding plots of the Q-band data, restricted to the $\tilde{a}$ axis, are presented as insets. In the whole temperature range (4.2 K–300 K) the linewidth and the g shift exhibit a behavior very similar to the X-band results. Also, the absolute values for both compounds show no significant frequency dependence.

IV. ANALYSIS AND DISCUSSION

A. Charge-ordered state

1. Temperature- and angular-dependent linewidth

At T_{CO} we observe interesting modifications in the linewidth (top panels of Figs. 4 to 8) that are analyzed in more detail in the following. For the $(TMTTF)_2SbF_6$ and $(TMTTF)_2AsF_6$ crystals, $\Delta H(T)$ decreases more slowly upon entering the CO state; for $(TMTTF)_2SCN$ it even increases at lower temperatures. Also the anisotropy of the linewidth changes in the ordered region with important differences between the salts with centrosymmetrical anions and those with linear anions. These observations indicate that the broadening mechanism below T_{CO} is different from the mechanism above. To give a clearer picture of the effect induced by CO, we define

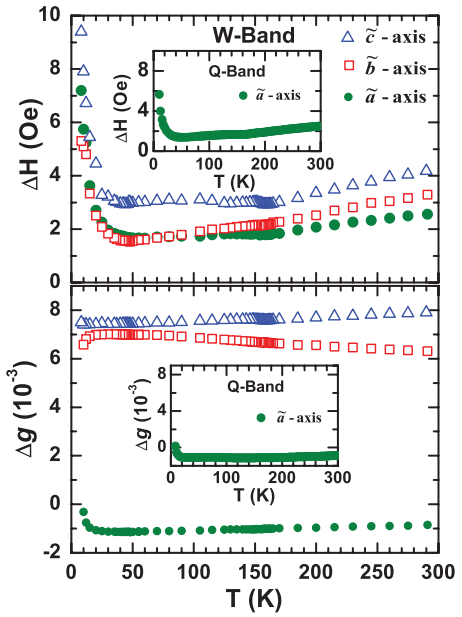

FIG. 7. (Color online) Temperature dependence of the W-band ESR linewidth and the g shift of $(TMTTF)_2SbF_6$ along the three principal magnetic axes $\tilde{a}$, $\tilde{b}$, and $\tilde{c}$. The insets show the ESR linewidth and the g shift measured in the Q-band spectrometer along the $\tilde{a}$ axis. The solid green dots correspond to the $\tilde{a}$ axis, the open red squares to the $\tilde{b}$ direction, and the open blue triangles to the $\tilde{c}$ axis.

the change of the linewidth by

$$\Delta H_{\mathrm{CO}}(T) = \Delta H(T) - \Delta H_{\mathrm{background}}(T) \qquad (3)$$

for each $(TMTTF)_2X$ salt and the three principal directions $\tilde{a}$, $\tilde{b}$, and $\tilde{c}$; the results are displayed in Fig. 9. Here $\Delta H_{\mathrm{CO}}(T)$ is the excess linewidth caused by the CO, $\Delta H(T)$ is the

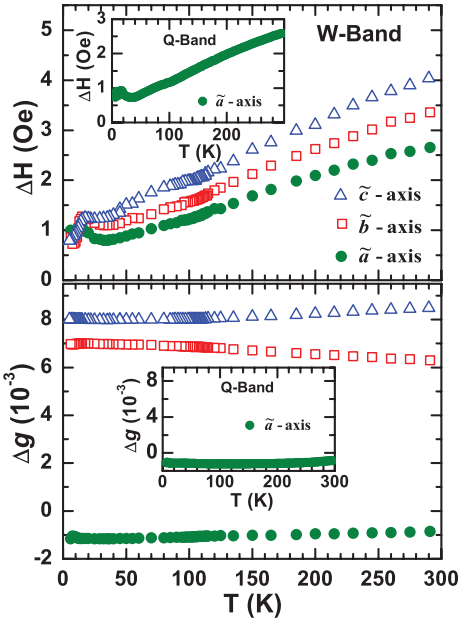

FIG. 8. (Color online) Temperature dependence of the W-band ESR linewidth and the g shift of $(TMTTF)_2AsF_6$ along the three axes $\tilde{a}$, $\tilde{b}$, and $\tilde{c}$. The Q-band ESR linewidth and the g shift ($\tilde{a}$ axis) are displayed in the insets, respectively.

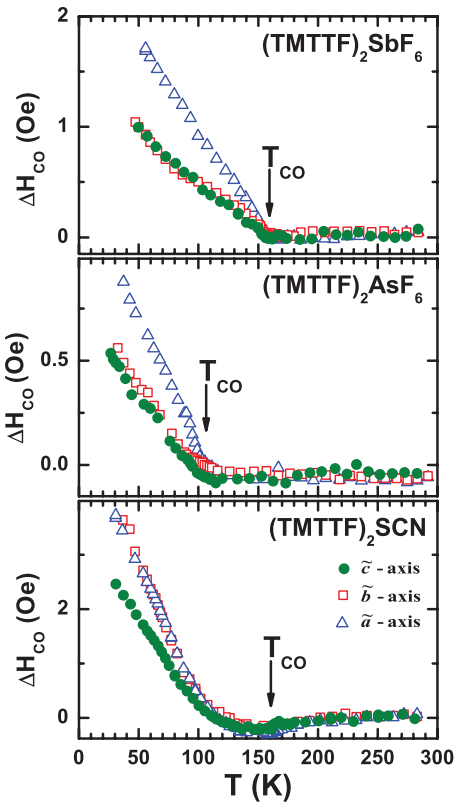

FIG. 9. (Color online) Contributions to the ESR linewidth due to CO for the salts $(TMTTF)_2X$ ($X = SbF_6$, AsF_6, and SCN) along the three main axes. Note the different scales of ΔH_{CO}. The excess linewidth $\Delta H_{\mathrm{CO}}(T)$ is given by $\Delta H(T) - \Delta H_{\mathrm{background}}(T)$ and explained in the text. Note, the data are shown for temperatures well above the magnetic ordering and spin Peierls transitions that occur for $T < 20$ K.

linewidth actually measured. To estimate $\Delta H_{\mathrm{background}}(T)$ we have chosen $(TMTTF)_2PF_6$ because the compound orders only at $T_{\mathrm{CO}} = 67$ K and even then exhibits only minor changes. For $T \geqslant 30$ K the effect on the linewidth is marginal, as can be seen from Fig. 12. Normalizing the data displayed in Fig. 3(a) to the respective room-temperature values ΔH of the investigated salts, we can use it as anisotropic and temperature-dependent background and avoid any offset.

As seen from Fig. 9, ΔH_{CO} equals zero for $T > T_{\mathrm{CO}}$ but begins to increase below the CO temperature. There is a distinct difference between the salts with centrosymmetrical and non-centrosymmetric anions. For $(TMTTF)_2SbF_6$ and $(TMTTF)_2AsF_6$ the linewidth changes abruptly at T_{CO}, while a gradual transition is found in $(TMTTF)_2SCN$. As far as the absolute values are concerned, the CO contribution to the linewidth, ΔH_{CO}, is smaller for $(TMTTF)_2AsF_6$ compared to $(TMTTF)_2SbF_6$ by about a factor of 2. This indicates a higher degree of charge disproportionation in $(TMTTF)_2SbF_6$, in agreement with conclusions drawn from NMR[20] and infrared measurements.[32,33] In $(TMTTF)_2SCN$ we find $\Delta H_{\tilde{a}} < \Delta H_{\tilde{b}} = \Delta H_{\tilde{c}}$, which is distinct from the anisotropy measured concordantly for both centrosymmetric compounds: $\Delta H_{\tilde{a}} = \Delta H_{\tilde{b}} < \Delta H_{\tilde{c}}$.

Adrian showed theoretically[53] that the TMTTF molecules are subject to torsional oscillations around their long molecular

$\tilde{c}$ axis that can cause spin-orbit scattering. However, symmetry arguments exclude intrastack spin-orbit scattering of a magnitude comparable to the interstack scattering. Electronic transitions within the stacks are not possible between identically oriented, centrosymmetric donor molecules. Hence, the inversion symmetry present in the crystals above T_{CO} precludes intrastack spin-orbit scattering in the TMTTF chains. For that reason, the anisotropy of the ESR linewidth ($\Delta H_{\tilde{a}} < \Delta H_{\tilde{b}} < \Delta H_{\tilde{c}}$) does not change with temperature at $T > T_{CO}$.

The significant modifications in $\Delta H(T)$ noted for $T < T_{CO}$ indicate dramatic changes in symmetry. Also dielectric permittivity[15–17] and NMR measurements[9,18,20] as well as second-harmonic generation[54] led to the conclusion that the TMTTF molecules in the stacks are not connected any more by inversion centers due to CO. The loss of symmetry below T_{CO} allows spin-orbit scattering in the TMTTF chains to increase and to contribute appreciably to the linewidth. With decreasing temperature the excess $\Delta H_{CO}(T)$ increases and its anisotropy becomes more significant. The difference in $\Delta H_{CO}(T)$ observed for the salts with centrosymmetric anions compared to non-centrosymmetric anions indicates that not only charge disproportionation is important in this regard. Hence, we conclude that the CO pattern[55] also depends on the symmetry of the counterions, in accord with previous ESR investigations by Nakamura.[21,34] In the case of $(TMTTF)_2SCN$ the CO occurs simultaneously with the ordering of the anions. While x-ray investigations reveal a superstructure along the b and c directions, no corresponding indications have been observed in crystals with centrosymmetric anions.[37]

Nakamura argues that the angular-dependent linewidth results from intersite magnetic dipole-dipole coupling, and consequently angular studies of the linewidth will reveal details of the CO arrangement.[21] Hence, we performed detailed angular-dependent measurements of ΔH and Δg for the investigated salts along the three planes $\tilde{a}\tilde{b}$, $\tilde{a}\tilde{c}$, and $\tilde{b}\tilde{c}$ at different temperatures above and below T_{CO}. In all cases the angular dependence of the g value remains unchanged with temperature and corresponds to the orientational dependence as displayed in the lower frame of Fig. 2 for $T = 300$ K. Also, the linewidth does not change its angular dependence within the $\tilde{a}\tilde{c}$ and $\tilde{b}\tilde{c}$ planes at low temperatures. Important deviations, however, are observed for the linewidth below T_{CO} when measured in the $\tilde{a}\tilde{b}$ plane. As already pointed out in Figs. 4 and 5, $\Delta H(\theta)$ becomes basically identical for the $\tilde{a}$ and $\tilde{b}$ axes of $(TMTTF)_2SbF_6$ and $(TMTTF)_2AsF_6$. Accordingly, when measured within this plane, the anisotropy in $\Delta H(\theta)$ should vanish in the CO state. Surprisingly Figs. 10 and 11 demonstrate some characteristic changes in the orientation dependence of the linewidth for the two salts. For $T > T_{CO}$, $\Delta H(\theta)$ is smallest along the stacks ($\tilde{a}$ axis, $\theta = 0°$) and largest perpendicular to it ($\tilde{b}$ axis, $\theta = 90°$). Upon entering the CO region ($T < T_{CO}$), maxima in the orientational pattern appear at the intermediate angles $\theta = 45°$ and $135°$ within the $\tilde{a}\tilde{b}$ plane, while for $\theta = 90°$ a minimum develops that becomes as low as for $\theta = 0°$ at low temperatures. The two maxima in the diagonal directions are more pronounced at low temperatures and enhanced for the Q-band and even more for the W-band measurements.[56] Such a behavior was not found in $(TMTTF)_2SCN$, as is shown later in Fig. 16.

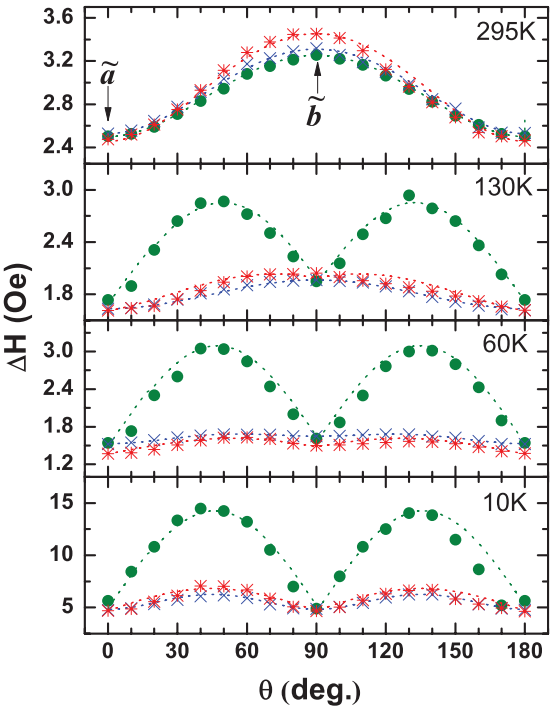

FIG. 10. (Color online) Angular dependence of the ESR linewidth within the $\tilde{a}\tilde{b}$ plane of $(TMTTF)_2SbF_6$ measured at different temperatures above and below the CO transition $T_{CO} = 156$ K using X-band (blue crosses), Q-band (red stars), and W-band (green dots) spectrometers. The lines represent fits of the linewidth using Eqs. (4) and (5) (see text for more details).

In the case of $(TMTTF)_2PF_6$ the CO transition takes place at considerably lower temperatures ($T_{CO} = 67$ K). We did not acquire a complete set of data at different temperatures and frequencies, but only X-band measurements at $T = 30$ K; from those we were able to extract the enhanced linewidth $\Delta H_{en} = 0.085$ Oe.[57] In Fig. 12 the angular-dependent linewidth of $(TMTTF)_2PF_6$ taken at different temperatures is plotted for the $\tilde{a}\tilde{b}$ plane. The doubling of the periodicity can be clearly seen at 19 K.

Following Eq. (1) above T_{CO} the angular dependence of $\Delta H(\theta)$ for the salts with centrosymmetric anions $(TMTTF)_2SbF_6$, $(TMTTF)_2AsF_6$, and also $(TMTTF)_2PF_6$ can be modeled by

$$\Delta H_{sp}(\theta) = \left[\Delta H_{sp}^2(\tilde{a})\cos^2\theta + \Delta H_{sp}^2(\tilde{b})\sin^2\theta\right]^{1/2}, \quad (4)$$

where $\Delta H_{sp}(\tilde{a})$ and $\Delta H_{sp}(\tilde{b})$ are the linewidths induced by spin-phonon scattering along the $\tilde{a}$ and $\tilde{b}$ axes, respectively, and θ is the angle between B_0 and the $\tilde{a}$ axis. In the CO state the orientational dependence of the linewidth can be fitted by the sum of Eqs. (4) and (5):

$$\Delta H_{mod}(\theta) = \Delta H_{mod}(45°)|\sin\{2\theta\}|. \quad (5)$$

In other words, a new broadening mechanism appears for $T < T_{CO}$ that causes a doubling of the periodicity of $\Delta H(\theta)$ within the $\tilde{a}\tilde{b}$ plane. Since the doubling is not found in $(TMTTF)_2SCN$, this effect seems to be confined to those systems which show no anion ordering simultaneously with the CO. The parameters obtained from the fit of the angular

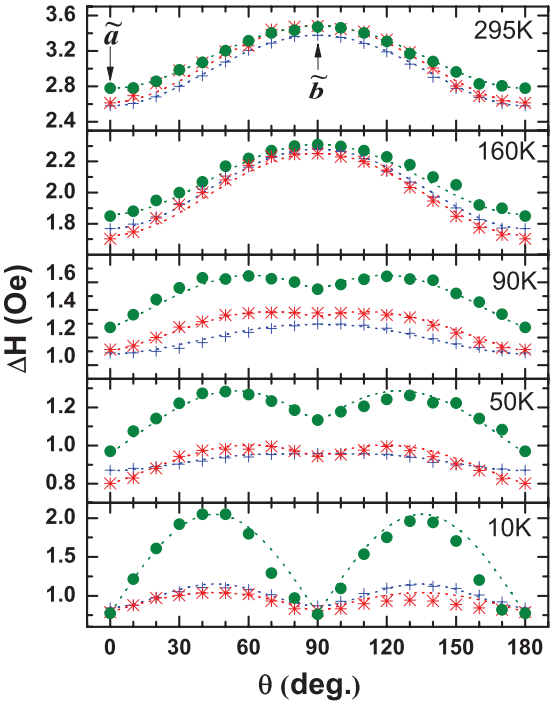

FIG. 11. (Color online) Angular dependence of the X-band (blue crosses), Q-band (red stars), and W-band (green dots) ESR linewidth when rotated along the $\tilde{a}\tilde{b}$ plane measured in $(TMTTF)_2AsF_6$ (T_{CO} = 102 K) at different temperatures, as indicated in the frames. The lines represent fits of ΔH using Eqs. (4) or (5).

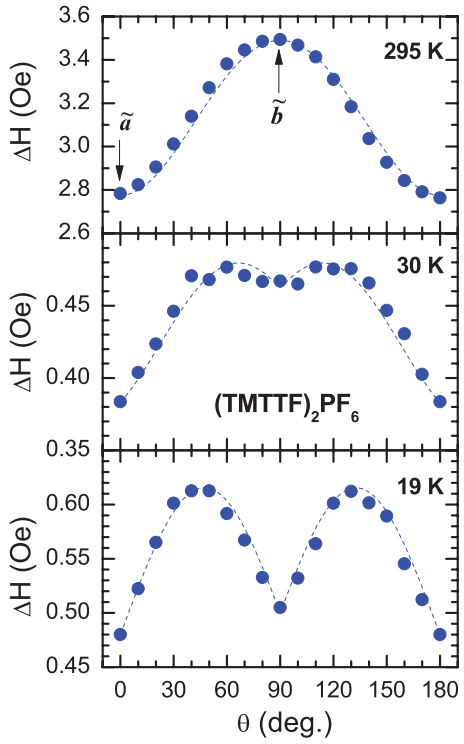

FIG. 12. (Color online) Angular dependence of the ESR linewidth within the $\tilde{a}\tilde{b}$ plane of $(TMTTF)_2PF_6$ measured at different temperatures T = 295 K, 30 K, and 19 K using an X-band spectrometer. The line represents a fit of the linewidth using Eqs. (4) and (5).

dependence of $\Delta H(\theta,T)$ at different temperatures T are listed in Table III for the three spectroscopic frequencies, X-band, Q-band, and W-band. A significant frequency dependence of the linewidth is observed only below T_{CO}, and this effect is in particular enhanced along the diagonal directions ($\theta = 45^\circ$ and 135°) of the $\tilde{a}\tilde{b}$ plane. We conclude that the new broadening mechanism, which causes the periodicity of the linewidth to double within the $\tilde{a}\tilde{b}$ plane, strongly depends on frequency.

2. *Anisotropic Zeeman interaction*

To understand better the nature of the line broadening in the CO state, let us consider in more detail the frequency dependence observed for $(TMTTF)_2SbF_6$ and $(TMTTF)_2AsF_6$. The enhanced linewidth ΔH_{en} along $\theta = 45^\circ$ in the $\tilde{a}\tilde{b}$ plane can be calculated for the X-, Q- and W-bands using[58]

$$\Delta H_{en} = \Delta H(45^\circ) - \tfrac{1}{2}[\Delta H(\tilde{a}) + \Delta H(\tilde{b})], \qquad (6)$$

where $\Delta H(45^\circ)$ is the linewidth along the 45° direction in $\tilde{a}\tilde{b}$ plane. The calculated values of ΔH_{en} for both salts at different temperatures $T < T_{CO}$ are plotted versus frequency in Fig. 13. In both compounds measured, ΔH_{en} rises slightly when the frequency increases from 9.5 GHz (X band) to 34 GHz (Q band) and exhibits a strong upturn when going to 95 GHz (W band).[56] The frequency dependence is consistent with quadratic behavior:

$$\Delta H_{en}(\nu) = A + B\nu^2, \qquad (7)$$

where A and B are fit parameters. In combination with the observed temperature dependence this result is a strong indication of the anisotropic Zeeman (AZ) interaction[59] and rules out Dzyaloshinskii-Moriya exchange interaction as an alternative explanation.[60] We can clearly state that our findings are inconsistent with a previous suggestion[21] of intersite magnetic dipole coupling.

Pilawa[61] and Heinrich *et al.*[62] report a similar behavior for the inorganic quasi-one-dimensional $S = \frac{1}{2}$ AFM Heisenberg systems $CuGeO_3$ and $CuSb_2O_6$; that is, the linewidth doubles its periodicity upon rotation in the plane. Their observations are explained by the coexistence of two magnetically inequivalent, exchange coupled Cu^{2+} sites in the systems. The analogy to our findings infers that also in the TMTTF compounds charge disproportionation leads to nonequivalent magnetic sites. We come back to this issue below (Sec. IV A3).

Let us first proceed analyzing our results on $(TMTTF)_2SbF_6$ in the framework of the theory of exchange-narrowed ESR spectra.[59] The contribution of the AZ interaction to the ESR linewidth can be approximated by[61]

$$\frac{\Delta H_{AZ}}{H_0} \approx \frac{g_e \mu_B H_0}{k_B |J'|} \sqrt{\frac{\pi}{8}} \left|\frac{\delta g}{g_e}\right|^2, \qquad (8)$$

where J' is the exchange interaction constant between the two inequivalent magnetic sites on the neighboring chains and δg is the difference between the **g** tensors of the two inequivalent magnetic sites. Four remarks should be made regarding Eq. (8): (i) In his derivation Pilawa uses a factor of 2 in the Hamiltonian for the interchain exchange interaction $\propto 2J' S_i S_j$, while many papers in TMTTF compounds are based on an exchange Hamiltonian $\propto J S_i S_j$. For the example of $(TMTTF)_2SbF_6$, the interchain exchange constant to

TABLE III. Parameters for the angular dependence of the linewidth measured along the $\tilde{a}\tilde{b}$ plane of $(TMTTF)_2SbF_6$ and $(TMTTF)_2AsF_6$ at different temperatures above and below the CO transitions $T_{CO} = 156$ K and 102 K, respectively. The values are obtained by modeling the data according to Eqs. (4) and (5).

	X band			*Q* band			*W* band		
T (K)	$\Delta H(\tilde{a})$ (Oe)	$\Delta H(\tilde{b})$ (Oe)	$\Delta H_{mod}(45^\circ)$ (Oe)	$\Delta H(\tilde{a})$ (Oe)	$\Delta H(\tilde{b})$ (Oe)	$\Delta H_{mod}(45^\circ)$ (Oe)	$\Delta H(\tilde{a})$ (Oe)	$\Delta H(\tilde{b})$ (Oe)	$\Delta H_{mod}(45^\circ)$ (Oe)
				$(TMTTF)_2SbF_6$					
295	2.53	3.31	0	2.46	3.45	0	2.58	3.37	0
130	1.61	1.96	0.03	1.61	1.99	0.13	1.69	1.95	1.02
60	1.52	1.64	0.08	1.37	1.48	0.18	1.48	1.60	1.55
10	4.82	4.82	1.38	4.69	4.69	2.13	4.90	4.90	9.35
				$(TMTTF)_2AsF_6$					
295	2.58	3.37	0	2.62	3.49	0	2.78	3.48	0
160	1.76	2.28	0	1.73	2.25	0	1.86	2.31	0
90	1.10	1.29	0.01	1.1	1.35	0.10	1.27	1.54	0.20
50	0.87	0.95	0.03	0.8	0.94	0.11	0.96	1.12	0.23
10	0.85	0.85	0.27	0.79	0.79	0.25	0.77	0.77	1.28

be used in Eq. (8) is therefore estimated as $J' = 1.1$ K.[63] We adopt this value also for $(TMTTF)_2AsF_6$ and $(TMTTF)_2PF_6$ which have the same crystal structure and J value. (ii) Equation (8) is simplified compared to Pilawa's original expression, because at 95 GHz—where the AZ effect can be reliably evaluated—the contribution of the nondiagonal elements of the **g** tensor can be neglected as it is reduced by one order of magnitude due to the exponential factor. (iii) In $CuGeO_3$ and $CuSb_2O_6$ the inequivalent sites are located on adjacent chains. Also for the TMTTF salts the narrowing of the line is caused not by intrastack exchange but by the interstack exchange constant, for the interaction within the stacks is so large that it would suppress the AZ effect in the frequency range under consideration. Thus, we conclude that the magnetically nonequivalent sites are situated on different TMTTF stacks. (iv) For that reason, the situation observed in our systems is distinct from alternating chains with two magnetically distinct sites, such as copper benzoate.[64–66] For $(TMTTF)_2X$ all dimers on a chain should be magnetically equivalent.

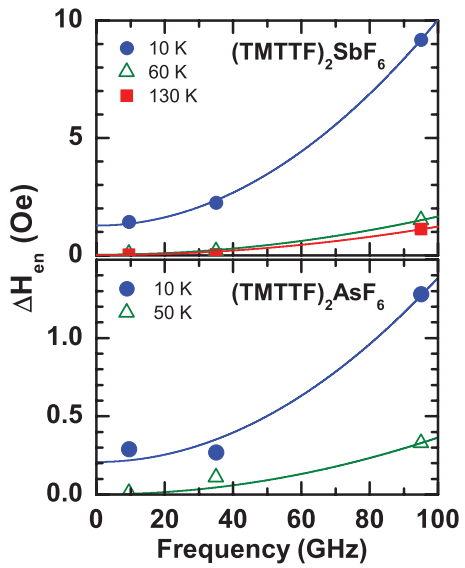

FIG. 13. (Color online) Frequency dependence of the enhanced ESR linewidth ΔH_{en} measured in the $\tilde{a}\tilde{b}$ plane along the diagonal direction ($\theta = 45^\circ$). The data for $(TMTTF)_2SbF_6$ are shown at $T =$ 10 K (blue dots), 60 K (green triangles), and 130 K (red squares) for $(TMTTF)_2AsF_6$ at 10 K (blue dots) and 50 K (green triangles). The lines are fits using Eq. (7).

From Eq. (8) we can calculate the difference between the **g** tensors of the two inequivalent magnetic sites that develop for $T < T_{CO}$. Here δg is estimated using $\Delta H_{AZ} \rightarrow \Delta H_{en} = 1.55$ Oe at $\theta = 45^\circ$ for the *W* band and at $T = 60$ K, that is, where the high-temperature approximation $T \gg J'$ anticipated for the derivation of Eq. (8) is valid.[67] With $J' = 1.1$ K and the resonance field $B_0 = 33\,600$ Oe we obtain $\delta g = 0.016\,78$ for $(TMTTF)_2SbF_6$.

The fact that the maximum of ΔH occurs at the diagonal direction $\theta = 45^\circ$ of the ab plane together with the finite δg value allows us to draw several important conclusions. The **g** tensors of the spins corresponding to the two different magnetic sites do not coincide with the principal magnetic axes but are rotated around the $\tilde{c}$ axis by ϕ in opposite directions, as depicted in Fig. 1. From Fig. 14 it becomes obvious that the anisotropy of the g value observed in the $\tilde{a}\tilde{b}$ plane is the sum of the contributions from the two different sites. The anisotropy of the g value for each magnetic site can be expressed by

$$g_1 = \left(g_{min}^2 \cos^2\{\theta - \phi\} + g_{max}^2 \sin^2\{\theta - \phi\}\right)^{1/2}, \quad (9a)$$

$$g_2 = \left(g_{max}^2 \cos^2\{\theta + \phi\} + g_{min}^2 \sin^2\{\theta + \phi\}\right)^{1/2}, \quad (9b)$$

where g_1 and g_2 correspond to the **g** tensor of type 1 and type 2 spins, respectively. The principal axes of the two kinds of spins span the angle 2ϕ. g_{max} and g_{min} are the maximum and the minimum of the g values for each kind of spins at the angle ϕ, respectively. For symmetry reasons the g values have to be identical $g_1 = g_2$ at $\theta = 0^\circ$ and $\theta = 90^\circ$, while at $\theta = 45^\circ$ the difference of the g values ($\delta g = 0.016\,78$) is obtained from the AZ effect. These conditions determine

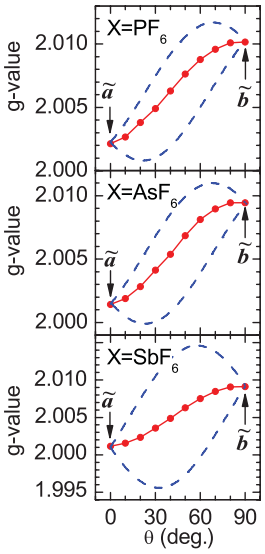

FIG. 14. (Color online) Angular dependence of the g value of $(TMTTF)_2PF_6$, $(TMTTF)_2AsF_6$, and $(TMTTF)_2SbF_6$ single crystals determined at $T = 29$ K, 50 K, and 60 K, respectively; the static magnetic field B_0 is rotated within the $\tilde{a}\tilde{b}$ plane, that is, perpendicular to the molecular axis as sketched in Fig. 1. The dotted lines indicate the calculated variation of the g value of the two magnetically inequivalent sites (g_1 and g_2) using Eq. (9).

three equations, which allow us to calculate $g_{\max} = 2.0143$, $g_{\min} = 1.9956$, and $2\phi = 64.5^\circ$, for the example of $(TMTTF)_2SbF_6$. In Table IV the results are listed for the various compounds.[68]

A few final remarks on the validity of Eq. (8) are in order. In case of AZ interaction, the ESR spectrum results from two different magnetic species in the single crystal. Let ν_{12} be the hopping rate between the two nonequivalent sites coupled by the interchain exchange interaction J'; then two extreme cases can be distinguished[69]: (i) In the weak coupling limit $\nu_{12} \ll |\nu_2 - \nu_1|$, where ν_i is the Larmor frequency of the species $i = 1,2$ two separated signals are present, leading to two distinct ESR lines. (ii) When $\nu_{12} \gg |\nu_2 - \nu_1|$ (strong coupling limit) only one single ESR signal is observed. The **g** tensor and the linewidth are then the weighted average between the characteristics of each magnetic species.

Comparing the energy scale of the interchain exchange coupling $J' = 1.1$ K and the difference of the Larmor frequencies in the W-band $\Delta\nu = (\Delta g/g) \times 95$ GHz (corresponding to $h\Delta\nu/k_B = 27$ mK), we clearly deal with case (ii) of strong coupling and, hence, the two signals merge into a single Lorentzian line, as observed in the experiment.[70] The linewidth is largest in the diagonal directions at 45° and 135°, where the AZ interaction produces the maximal broadening.[71]

Also in the inorganic Heisenberg system $CuGeO_3$, Pilawa could not resolve two separate lines up to 245 GHz because the interchain exchange constant of the two magnetically inequivalent Cu^{2+} sites is even larger: $J' = 4.2$ K.[61]

TABLE IV. Rotation of the **g** tensors $\pm\phi$ of two magnetically nonequivalent sites in adjacent stacks, as obtained from the fit of the angular-dependent data by Eq. (9) at $T \approx T_{CO}/2$. $g_{\max}$ and $g_{\min}$ is the maximum and the minimum of the g values for each kind of spin at the angle ϕ, respectively. δg is the difference of the g values at $\theta = 45^\circ$.

Compound	2ϕ (degrees)	$g_{\max}$	$g_{\min}$	δg (10^{-3})
$(TMTTF)_2PF_6$	44.0	2.0117	2.0008	7.45
$(TMTTF)_2AsF_6$	44.0	2.0071	1.9999	7.82
$(TMTTF)_2SbF_6$	64.5	2.0143	1.9956	16.8

3. *Charge order*

Charge order is driven by Coulomb repulsion of the electrons: The charges on different sites rearrange upon lowering the temperature leading to a disproportionation and ordering along the molecular chains; interchain interaction can eventually form a superlattice in all three directions.[13,72] In the case of $(TMTTF)_2X$ the charge on the TMTTF molecule changes from a homogeneous distribution with $\rho = 0.5e$ above T_{CO} to a modulated structure along the stacks $\rho = 0.5e \pm \delta$, with $\delta = 0.08e$ for $(TMTTF)_2PF_6$, $\delta = 0.11e$ for $(TMTTF)_2AsF_6$, and $\delta = 0.14e$ for $(TMTTF)_2SbF_6$, as determined by vibrational spectroscopy.[22,23,32,33]

While NMR and vibrational studies locally probe the nuclei or intramolecular bonds on a TMTTF molecule, ESR spectroscopy measures the electron distributed on a dimer. Due to the comparably strong intrastack coupling $J \approx 400$ K (Table I) we can basically assign a single **g** tensor to each stack. If CO just implies a charge imbalance within the dimer, this will not lead to a change in the **g** tensor. This is exactly what we find in the $\Delta g(T)$ behavior displayed in Figs. 3 to 5. There is, however, a coupling to the neighboring stacks, which is probably larger than the above-given $J' = 1.1$ K. The interstack coupling is not due to magnetic dipole-dipole coupling, as suggested by Nakamura,[21] but due to anisotropic Zeeman interaction.

At elevated temperatures inversion symmetry (with the center located at the anion, for instance) requires that the contacts I and II depicted in Fig. 1 are identical. It was shown[6,7] that not the distances to the methyl groups, but to the chalcogenides is crucial for the electronic coupling of anions and cations. For $T < T_{CO}$ the Coulomb attraction between organic molecules and anions becomes imbalanced, which on the one hand causes a distortion of the anions that makes the distances I and II in Fig. 1 unequal. On the other hand, the Coulomb potential of the anions influences the electronic wave function on the TMTTF molecules[9,40] in different ways depending on charge-rich and charge-poor molecules. This implies that also the spin density is affected at T_{CO}.

The $(TMTTF)_2X$ salts are $\frac{1}{4}$-filled systems with a slight dimerization along the stacks. Thus, there are two possible arrangements of charge-rich and charge-poor sites: $+-+-$ $+-$ (abbreviated by "l") or $-+-+-+$ (labeled "r").[73] We suggest that at the CO transition ferroelectric domains develop on the nanometer scale, as suggested by the increasing mosaicity observed in our x-ray results.[37] Due to the strong intrastack coupling we can assign one **g** tensor to each stack, which is rotated either in one ("l") or the other ("r") way, respectively. At the domain boundaries with opposite

polarization the interaction leads to a coupling of adjacent stacks with two inequivalent magnetic sites.

Without any coupling two distinct ESR signals would be expected below the ordering temperature T_{CO}, but the strong coupling leads to a significant broadening. As the averaged **g** tensor does not abruptly change at the phase transition, the effect of CO can be pictured as follows: Above T_{CO} random charge disproportionation exists on the TMTTF chains, giving rise to an averaged **g** tensor as observed, but without any AZ effect, which is suppressed due to the narrowing by large intrachain exchange. Below T_{CO}, the charge disproportionation becomes cooperative within each domain and at the boundaries adjacent chains weakly interact. This gives rise to two inequivalent sites that yield the same averaged **g** tensor as above T_{CO}, but the AZ effect becomes visible because the signal is narrowed by the much weaker interchain exchange.

Note that the splitting into two **g** tensors rotated by $\pm 32.25^\circ$ around the $\tilde{c}$ axis (see Fig. 1) that sets in at T_{CO} is distinct from the gradual uniform rotation of the **g** tensor around the $\tilde{a}$ axis as temperature decreases, which has recently been reported by Furukawa *et al.*[40] In $(TMTTF)_2SbF_6$, for example, the rotation angle around the $\tilde{a}$ axis at $T = 60$ K is equal to 13°, but as all sites exhibit the same rotation, it does not give rise to additional line broadening from AZ effect. Nevertheless, an indication of the rotation of the **g** tensor is given by Figs. 4 and 5, where the change in the anisotropy of the g value in the $\tilde{b}\tilde{c}$ plane with reduced temperature is seen.

Already, Riera and Poilblanc[74] suggested that CO in TMTTF salts is a cooperative effect between the Coulomb interaction and the electronic coupling of the TMTTF stacks to the anions; small displacements of the anions along some arbitrary directions lead to local changes of the on-site electronic energies which produce nonequivalent magnetic sites. We conclude from our ESR measurements that in the CO regime two inequivalent magnetic TMTTF sites coexist on neighboring stacks, which produce a doubling in the angular periodicity of the linewidth as well as the characteristic quadratic frequency dependence.

We should note that for the lowest temperature presented in Fig. 10, $(TMTTF)_2SbF_6$ approaches the antiferromagnetic order at $T_N = 8$ K. In the subsequent Sec. IV B we discuss the fluctuation regime in more detail. We note that for $(TMTTF)_2SbF_6$ the linewidth increases by a factor of 6 in the fluctuation regime. Looking at Eq. (8) this implies a decrease of $|J'|$ or—more likely—an increase of δg by a factor of 2.5. In Figs. 11 and 12 we present data of $(TMTTF)_2AsF_6$ and $(TMTTF)_2PF_6$ in the spin-Peierls state. It seems that the CO state is not affected by the spin-Peierls transition.

B. Antiferromagnetic fluctuations

Let us come back to the temperature dependence of the linewidth as displayed in Figs. 4 and 6. As the temperature is reduced and approaches the AFM ordering $T_N = 8$ K and 7 K of $(TMTTF)_2SbF_6$ and $(TMTTF)_2SCN$, respectively, $\Delta H(T)$ strongly increases. This singularity of the ESR linewidth is a signature of magnetic fluctuations. Bourbonnais presented a detailed theoretical analysis of $\Delta H(T)$ in the AFM fluctuation region.[75] In the case of a small static magnetic field B_0,

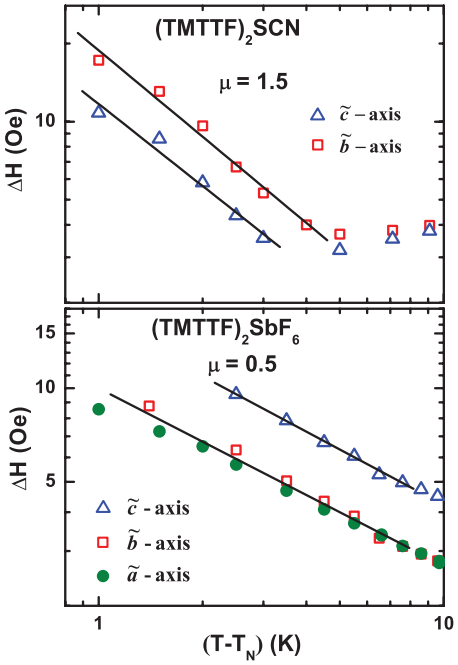

FIG. 15. (Color online) Double-logarithmic plot of the linewidth versus $T - T_N$ of $(TMTTF)_2SCN$ (top) and $(TMTTF)_2SbF_6$ (bottom) in the antiferromagnetic fluctuation region; the X-band data are taken at different directions, as indicated. The lines represent the fit to a power law $\Delta H(T) \propto (T - T_N)^{-\mu}$ given in Eq. (10) with the exponent $\mu = 1.5$ for $(TMTTF)_2SCN$ and $\mu = 0.5$ for $(TMTTF)_2SbF_6$, where $T_N = 7$ K in the case of $(TMTTF)_2SCN$ and 8 K for $(TMTTF)_2SbF_6$.

the linewidth in the fluctuation region follows a power-law behavior:

$$\Delta H(T \to T_N) \propto \left(\frac{T - T_N}{T_N}\right)^{-\mu}, \tag{10}$$

where μ depends on the dimension d of the AFM fluctuations. If dipole-dipole interactions are the dominant relaxation process in this critical region, the exponent is given by $\mu = 3 - d/2$; that is, $\mu = 3/2$ is predicted for three-dimensional AFM fluctuations.[75]

In Fig. 15 we present the analysis of the temperature dependence of ΔH for the two materials investigated near the AFM phase transition. The data of $(TMTTF)_2SCN$ follow the power-law given by Eq. (10) with $\mu = 1.5$ expected for fluctuations associated with three-dimensional AFM ordering below T_N. Both directions ($B_0 \parallel \tilde{b}$ and $B_0 \parallel \tilde{c}$) exhibit the same behavior. Our findings are in agreement with previous NMR investigations where a critical behavior in the relaxation rate was reported.[76] The same slope of $\Delta H(T)$ with $\mu = 1.5$ was found in the AFM fluctuation region of $(TMTSF)_2PF_6$, $(TMTSF)_2AsF_6$, and $(TMTTF)_2Br$.[49,50,77,78]

Surprisingly, a different power law of $\mu = 0.5$ is obtained in the data of $(TMTTF)_2SbF_6$ where AZ interaction is present. This observation was made in all three directions and for all three frequencies used in our study. The reason might be the different anisotropy in the spin degree of freedom, but also the relative magnitude of the dipole-dipole interaction and spin-orbit interaction is different compared to $(TMTTF)_2SCN$. It seems that dipole-dipole interaction is missing at all in

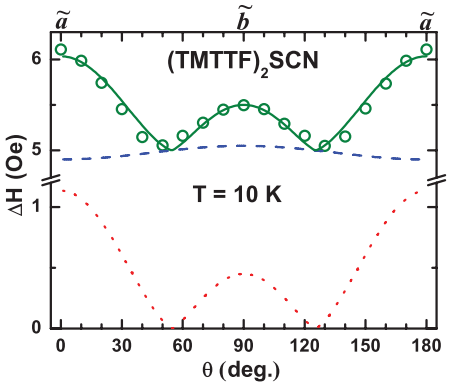

FIG. 16. (Color online) Angular dependence of the linewidth $\Delta H(\theta)$ of $(TMTTF)_2SCN$ measured in the X band along the $\tilde{a}\tilde{b}$ plane. The green open circles are data in the antiferromagnetic fluctuation region at $T = 10$ K. The red dotted line represents a fit of the dipole-dipole interaction with $\Delta H_{d-d} = \Delta H_{\tilde{b}}[3\cos^2\theta - 1]^{4/3}$, the blue dashed line a fit of the spin-phonon interaction by Eq. (4). The solid green line is the sum of both contributions and perfectly describes the data.

$(TMTTF)_2SbF_6$. It is interesting to note that results similar to $(TMTTF)_2SbF_6$ ($\mu = 0.5$) have been reported previously for $(TMTSF)_2NO_3$.[77] Further investigations seem to be necessary to get a complete picture of the behavior in the AFM fluctuation regime of these TMTTF salts with different anions.

The angular dependence of the linewidth of $(TMTTF)_2SCN$ within the $\tilde{a}\tilde{b}$ plane is displayed in Fig. 16. The data are measured in the AFM fluctuation region at $T = 10$ K. By rotating the crystal around the $\tilde{c}$ axis (B_0 normal to the molecular axis), the line is broadest along the $\tilde{a}$ direction ($\theta = 0°$) but $\Delta H(\theta)$ has only an intermediate value along the $\tilde{b}$ direction ($\theta = 90°$). The narrowest line is observed for $\theta = 55°$ and $125°$. Finding the minimum near the magic angle ($\theta = 54.7°$) is a strong indication that dipole-dipole interaction contributes significantly to the relaxation process in this range of temperature. If we assume dipole-dipole interaction to be the dominant relaxation process in one-dimensional systems, we expect for the angular dependence $\Delta H_{d-d}(\theta) = \Delta H_{\tilde{b}}[3\cos^2\theta - 1]^{4/3}$. As seen in Fig. 16 the orientational dependence of the linewidth of $(TMTTF)_2SCN$ at $T = 10$ K can be well fitted by adding the contributions of the dipole-dipole interaction and of the spin-phonon interaction. In other words, in the AFM fluctuation regime both interactions contribute to the relaxation process and produce a unique angular dependence of $\Delta H(\theta)$.

From Figs. 4 and 6 it can be seen that for both salts $(TMTTF)_2SCN$ and $(TMTTF)_2SbF_6$, the g values become strongly temperature dependent as T approaches the AFM ordering temperature T_N. With lowering the temperature $g(T)$ increases strongly along the $\tilde{a}$ axis, but drops for the $\tilde{b}$ and $\tilde{c}$ axes. Such a behavior is expected for AFM ordering when the environment of a given spin is modified by the magnetic correlations. The existence of a fluctuating local field causes a typical temperature dependence of the g factor: It increases along the hard axis and decreases along the intermediate and easy axes. In previous measurements of the antiferromagnetic resonance Coulon *et al.* could determine the hard, intermediate, and easy axes to be close to the $\tilde{a}$, $\tilde{c}$, and $\tilde{b}$ axes of the TMTTF salts, respectively.[79] Our observation of the temperature-dependent g value agrees perfectly with this assignment.

V. CONCLUSIONS

We have performed detailed multifrequency ESR investigations on single crystals of the organic spin-chain compounds $(TMTTF)_2X$ ($X = PF_6$, SbF_6, AsF_6, and SCN) in the temperature range from 4 K to 300 K. Particular emphasis was put on the charge-ordered states in these materials and the interaction of charge, spin, and lattice degrees of freedom. At high temperatures, all compounds have a distinct anisotropy and show a linear decrease of the linewidth with decreasing temperature; similar observations for the linewidth and the g value have been made for all three orientations. This behavior also does not depend on the applied microwave frequency (9.5, 34, and 95 GHz).

Charge order entails ferroelectric domains with opposite polarization on the nanometer scale. We could show that CO also significantly influences the magnetic behavior of the spin chain. For $T < T_{CO}$ the charge disproportionation on the TMTTF molecules leads to two nonequivalent couplings between the anions and the TMTTF molecules. This broken inversion symmetry of the $(TMTTF)_2X$ crystals causes a modification of the local structural arrangement that rotates the $\mathbf{g}$ tensor around the molecular axis by an angle $\pm\phi$. At the domain boundary two inequivalent magnetic sites interact and cause additional contributions ΔH_{en} to the ESR linewidth. When looking along the diagonal orientation of the $\tilde{a}\tilde{b}$ plane ($\theta = 45°$) the linewidth of $(TMTTF)_2SbF_6$ and $(TMTTF)_2AsF_6$ is strongly enhanced for the Q- and W-band measurements with a quadratic frequency dependence. This behavior is a strong indication for the anisotropic Zeeman effect. Since the interchain exchange is strong enough to narrow both signals into a single Lorentz line even at W-band frequencies, we do not observe any splitting of the ESR signal. Nevertheless, anisotropic Zeeman interaction is an important line-broadening mechanism in the charge-ordered state.

The anisotropy of the linewidth is found to be very different for compounds with the centrosymmetric anions and $(TMTTF)_2SCN$, which simultaneously undergoes an anion transition. The distinct angular dependence of the linewidth below T_{CO} gives evidence for different CO patterns in these compounds.

ACKNOWLEDGMENTS

We thank C. Bourbonnais, S. Brown, G. Denninger, A. Janossy, M. Mehring, and D. Schweitzer for useful discussions. S.Y. wants to thank H. J. Kümmerrer for assistance in performing the W-band ESR experiment. This work was supported by the Deutsche Forschungsgemeinschaft (DFG) via the Graduate College "Modern Methods of Magnetic Resonance in Materials Science" of the Stuttgart University and partially via the Transregional Collaborative Research Center TRR80 "From Electronic Correlations to Functionality" (Augsburg, München).

[1]D. Jérome and H. J. Schulz, Adv. Phys. **31**, 299 (1982).
[2]J. Moser, M. Gabay, P. Auban-Senzier, D. Jérome, K. Bechgaard, and J. M. Fabre, Eur. Phys. J. B **1**, 39 (1998).
[3]C. Bourbonnais and D. Jérome, in *Advances in Synthetic Metals*, edited by P. Bernier, S. Lefrant, and G. Bidan (Elsevier, Amsterdam, 1999), p. 206.
[4]M. Dressel, Naturwissenschaften **90**, 337 (2003); J. Phys.: Condens. Matter **23**, 293201 (2011).
[5]M. Dressel, Naturwissenschaften **94**, 527 (2007).
[6]B. Köhler, E. Rose, M. Dumm, G. Untereiner, and M. Dressel, Phys. Rev. B **84**, 035124 (2011).
[7]E. Rose and M. Dressel, Physica B **407**, 1787 (2012).
[8]J. P. Pouget and S. Ravy, J. Phys. I (France) **6**, 1501 (1996).
[9]W. Yu, F. Zhang, F. Zamborszky, B. Alavi, A. Baur, C. A. Merlic, and S. E. Brown, Phys. Rev. B **70**, 121101 (2004).
[10]D. Chasseau, J. Gaultier, J. L. Miane, C. Coulon, P. Delhaes, S. Flandrois, J. M. Fabre, and L. Giral, J. Phys. Colloq. (France) **44**, C3-1223 (1983).
[11]L. Ducasse, M. Abderrabba, B. Gallois, and D. Chasseau, Synth. Met. **19**, 327 (1987).
[12]T. Granier, B. Gallois, A. Fritsch, L. Ducasse, and C. Coulon, in *Lower Dimensional Systems and Molecular Electronics*, edited by R. M. Metzger, P. Day, and G. C. Papavassiliou (Plenum Press, New York, 1990), Vol. 248 of NATO ASI, Series B: Physics, p. 163.
[13]H. Seo and H. Fukuyama, J. Phys. Soc. Jpn. **66**, 1249 (1997).
[14]F. Nad, P. Monceau, and J. M. Fabre, Eur. Phys. J. B **3**, 301 (1998).
[15]F. Nad, P. Monceau, C. Carcel, and J. M. Fabre, J. Phys.: Condens. Matter **13**, L717 (2001).
[16]P. Monceau, F. Y. Nad, and S. Brazovskii, Phys. Rev. Lett. **86**, 4080 (2001).
[17]F. Nad and P. Monceau, J. Phys. IV (France) **12**, Pr9-133 (2002).
[18]D. S. Chow, F. Zamborszky, B. Alavi, D. J. Tantillo, A. Baur, C. A. Merlic, and S. E. Brown, Phys. Rev. Lett. **85**, 1698 (2000).
[19]F. Zamborszky, W. Yu, W. Raas, S. E. Brown, B. Alavi, C. A. Merlic, and A. Baur, Phys. Rev. B **66**, 081103(R) (2002).
[20]W. Yu, F. Zamborszky, B. Alavi, A. Baur, C. A. Merlic, and S. E. Brown, J. Phys. IV (France) **114**, 35 (2004).
[21]T. Nakamura, J. Phys. Soc. Jpn. **72**, 213 (2003).
[22]M. Dumm, B. Salameh, M. Abaker, L. K. Montgomery, and M. Dressel, J. Phys. IV (France) **114**, 57 (2004).
[23]M. Dumm, M. Abaker, and M. Dressel, J. Phys. IV (France) **131**, 55 (2005).
[24]K. Furukawa, T. Hara, and T. Nakamura, J. Phys. Soc. Jpn. **74**, 3288 (2005).
[25]B. Korin-Hamzić, E. Tafra, M. Basletić, A. Hamzić, and M. Dressel, Phys. Rev. B **73**, 115102 (2006).
[26]S. Hirose, A. Kawamoto, N. Matsunaga, K. Nomura, K. Yamamoto, and K. Yakushi, Phys. Rev. B **81**, 205107 (2010).
[27]B. Salameh, S. Yasin, M. Dumm, G. Untereiner, L. Montgomery, and M. Dressel, Phys. Rev. B **83**, 205126 (2011).
[28]C. Coulon, S. S. P. Parkin, and R. Laversanne, Phys. Rev. B **31**, 3583 (1985).
[29]Sh. Fujiyama and T. Nakamura, Phys. Rev. B **70**, 045102 (2004).
[30]M. Dressel and N. Drichko, Chem. Rev. **104**, 5689 (2004).
[31]N. Drichko, S. Kaiser, Y. Sun, C. Clauss, M. Dressel, H. Mori, J. Schlueter, E. I. Zhyliaeva, S. A. Torunova, and R. N. Lyubovskaya, Physica B **404**, 490 (2009).
[32]T. Knoblauch and M. Dressel, Phys. Status Solidi C (2012) (in press).
[33]M. Dressel, M. Dumm, T. Knoblauch, and M. Masino, Crystals (2012) (in press).
[34]Y. Nogami and T. Nakamura, J. Phys. IV (France) **12**, Pr9-145 (2002).
[35]R. Laversanne, C. Coulon, B. Gallois, J. P. Pouget, and R. Moret, J. Phys. Lett. **45**, L393 (1984).
[36]S. Ravy, P. Foury-Leylekian, D. Le Bolloch, J. P. Pouget, J. M. Fabre, R. J. Prado, and P. Lagarde, J. Phys. IV **114**, 81 (2004).
[37]E. Rose, F. Lissner, T. Schleid, and M. Dressel (to be published).
[38]M. de Souza, P. Foury-Leylekian, A. Moradpour, J.-P. Pouget, and M. Lang, Phys. Rev. Lett. **101**, 216403 (2008).
[39]P. Foury-Leylekian, S. Petit, G. Andre, A. Moradpour, and J.-P. Pouget, Physica B **405**, 595 (2010).
[40]K. Furukawa, T. Hara, and T. Nakamura, J. Phys. Soc. Jpn. **78**, 104713 (2009).
[41]K. Furukawa, T. Hara, and T. Nakamura, J. Phys. Soc. Jpn. **79**, 043702 (2010).
[42]Complementary X-band measurements were performed at the Hochfeld-Magnetlabor Dresden and at the University Augsburg using a Bruker Elexsys 500 CW system.
[43]L. K. Montgomery, in *Organic Conductors*, edited by J. P. Farges (Dekker, New York, 1994), p. 138.
[44]A. Janossy (private communications).
[45]N. Kinoshita, T. Ukachi, M. Tokumoto, H. Anzai, T. Ishiguro, G. Saito, T. Yamabe, and H. Teramae, J. Phys. Colloq. C3 (France) **44**, C3-1029 (1983); N. Kinoshita, M. Tokumoto, H. Anzai, T. Ishiguro, G. Saito, T. Yamabe, and H. Teramae, J. Phys. Soc. Jpn. **53**, 1504 (1984).
[46]C. Coulon and R. Clérac, Chem. Rev. **104**, 5655 (2004).
[47]Previously, the long, intermediate, and short molecular axes have been heterogeneously labeled as x, y, and z (Ref. 45) or as c^*, b', and a axis (Ref. 50). Furukawa *et al*. and Kinoshita *et al*. indicated the principal axes of the **g** tensor as g_1, g_2, and g_3 (Refs. 40 and 45).
[48]M. Dressel, P. Hesse, S. Kirchner, G. Untereiner, M. Dumm, J. Hemberger, A. Loidl, and L. Montgomery, Synth. Met. **120**, 719 (2001).
[49]M. Dumm, A. Loidl, B. W. Fravel, K. P. Starkey, L. K. Montgomery, and M. Dressel, Phys. Rev. B **61**, 511 (2000).
[50]M. Dumm, A. Loidl, B. Alavi, K. P. Starkey, L. K. Montgomery, and M. Dressel, Phys. Rev. B **62**, 6512 (2000).
[51]C. P. Slichter, *Principle of Magnetic Resonance* (Springer-Verlag, Berlin, 1996).
[52]R. S. Drago, *Physical Methods in Chemistry* (Saunders, Philadelphia, 1977).
[53]F. J. Adrian, Phys. Rev. B **26**, 2682 (1982); **33**, 1537 (1986).
[54]K. Yamamoto, S. Iwai, N. Nishi, and K. Yakushi (unpublished).
[55]The CO pattern defines the arrangement of the charge-rich and charge-poor sites along the stacking axis a; these sites can be arranged in different ways, such as 1010 or 1001, for instance. See R. T. Clay, S. Mazumdar, and D. K. Campbell, Phys. Rev. B **67**, 115121 (2003).
[56]For $(TMTTF)_2AsF_6$ the X-band linewidth exceeds the Q-band data at $T = 10$ K. From Fig. 5 we can see that X-band data exhibit a strong temperature dependence in this range; for experimental reasons uncertainties in the absolute temperature value cannot be ruled out.
[57]We have calculated the enhanced linewidth at this temperature $T \approx 30$ K in order to eliminate any spin-Peierls fluctuation effects in our calculations.

[58]The enhanced linewidth (ΔH_{en}) for the Q- and W-band measurements is calculated by relating their linewidths along $\tilde{a}$ and $\tilde{b}$ axes to the ones of the X-band measurements in order to eliminate any sample-size effect in our calculations.

[59]A. Bencini and D. Gatteschi, in *Electron Paramagnetic Resonance of Exchange Coupled Systems* (Springer, Berlin, 1990).

[60]In the case of staggered fields, antisymmetric Dzyaloshinskii-Moriya interaction also causes a ω^2 frequency dependence of the linewidth; however, leading to a T^{-2} temperature dependence [H. Oshikawa and I. Affleck, Phys. Rev. Lett. **82**, 5136 (1999); H. Herak, A. Zorko, D. Arcon, A. Potocnik, M. Klanjsek, J. van Tol, A. Ozarowski, and H. Berger, Phys. Rev. B **84**, 184436 (2011)] in contrast to our findings. Note also that in those references Heisenberg spin chains with significant intra-chain Dzyaloshinskii-Moriya interaction were considered. In the present case, the alternating contributions result from interaction between the chains, for which the iostropic exchange J' is already small. Thus the antisymmetric Dzyaloshinskii-Moriya exchange can be neglected.

[61]B. Pilawa, J. Phys.: Condens. Matter **9**, 3779 (1997).

[62]M. Heinrich, H. A. Krug von Nidda, A. Krimmel, A. Loidl, R. M. Eremina, A. D. Ineev, B. I. Kochelaev, A. V. Prokofiev, and W. Assmus, Phys. Rev. B **67**, 224418 (2003).

[63]C. Yasuda, S. Todo, K. Hukushima, F. Alet, M. Keller, M. Troyer, and H. Takayama, Phys. Rev. Lett. **94**, 217201 (2005).

[64]M. Date, H. Yamazaki, M. Motokawa, and S. Tazawa, Prog. Theor. Phys. Suppl. **46**, 194 (1970).

[65]K. Okuda, H. Hata, and M. Date, J. Phys. Soc. Jpn. **33**, 1574 (1972).

[66]D. C. Dender, D. Davidović, D. H. Reich, C. Broholm, K. Lefmann, and G. Aeppli, Phys. Rev. B **53**, 2583 (1996).

[67]We have chosen this temperature $T \approx 60$ K in order to exclude antiferromagnetic fluctuation effects in our calculations.

[68]For $(TMTTF)_2AsF_6$ and $(TMTTF)_2SbF_6$ we see basically no increase in the enhanced linewidth when going from X band to Q band. A similar assumption can be made for $(TMTTF)_2PF_6$. For the analysis of the **g** tensor rotation; we have therefore used $B_0 = 1250$ Oe for the Q-band frequency.

[69]A. Carrington and A. D. McLachlan, *Introduction to Magnetic Resonance* (McLachlan, New York, 1967).

[70]We observe a slight distortion in the ESR spectra along the 45° and 135° below T_{CO}. It is known from previous studies that the distortion of the signal is a precursor of the splitting.

[71]E. I. Yudanova, S. K. Hoffmann, A. Graja, S. V. Konovalikhin, O. A. Dyachenko, R. B. Lubovskii, and R. N. Lyubovskaya, Synth. Met. **73**, 227 (1995).

[72]H. Seo, C. Hotta, and H. Fukuyama, Chem. Rev. **104**, 5005 (2004).

[73]There are no indications of a tetramerization along the stack, that is, an arrangement $+--++--+$.

[74]J. Riera and D. Poilblanc, Phys. Rev. B **63**, 241102 (2001).

[75]C. Bourbonnais, in *Interacting Electrons in Reduced Dimensions*, edited by D. Baeriswyl and D. K. Campdell (Plenum, New York, 1989), Vol. 213 of NATO ASI, Series B: Physics, p. 227.

[76]B. Liautard, S. Peytavin, G. Brun, and M. Maurin, J. Phys. Coll. C3 **44**, 951 (1983).

[77]S. Tomić, J. R. Cooper, W. Kang, D. Jérome, and K. Maki, J. Phys. I **1**, 1603 (1991).

[78]P. Baillargeon, C. Bourbonnais, S. Tomić, P. Vaca, and C. Coulon, Synth. Met. **27**, 83 (1988).

[79]C. Coulon, J. C. Scott, and R. Laversanne, Phys. Rev. B **33**, 6235 (1986).